Anastasiia Kutsenko[*]

PhD in Mathematics and Physics, Associate Professor
National University of Life and Environmental Sciences of Ukraine
03041, 15 Heroiv Oborony Str., Kyiv, Ukraine
https://orcid.org/0000-0003-1808-6773

Oleksii Kutsenko

PhD in Mathematics and Physics, Associate Professor
Taras Shevchenko National University of Kyiv
01033, 60 Volodymyrska Str., Kyiv, Ukraine
https://orcid.org/0000-0001-5089-0409

The gradual removal of Hertz pressure from the surface of elastic half-space

Abstract. Contact stress determination in non-stationary dynamic loading of elastic bodies is crucial for modelling structures at high speeds, but it presents mathematical challenges due to the time-dependent and often unknown contact area size and shape. The study aims to obtain an energy remainder estimation that forms waves during the contact interaction of elastic bodies, based on the exact solutions of non-stationary problems for an elastic half-space. For this purpose, the problem of the instantaneous loading half-space as an additional research problem was reconstructed using the Hankel transform concerning a radial coordinate and the Laplace transform concerning a time variable. The method of derivation of the displacements at an elastic half-space loaded (unloaded) gradually by Hertz's contact pressure has been proposed. Its availability made it possible to pass to the solution of the main problem – the problem of gradual loading of the half-space surface by Hertz pressure. The possibility of changing of the order of differentiation and integration operations in the obtained representation is substantiated based on the integrand properties. The cases when the speed of the indenter was constant when its motion was uniformly accelerated and when the motion corresponded to the law of the first quarter of the cosine period in the time were considered. It was concluded that the distribution of dynamic contact stresses is similar to the Hertz distribution. An estimation of the part of the energy spent on the formation of elastic waves was made for various laws of unloading. The practical significance of this study lies in its development of an effective method for calculating normal displacements on a loading area in dynamic contact interactions of elastic bodies, which can be valuable for modelling structures at high speeds

Keywords: dynamic contact interaction; refinement of the contact distribution; wave energy; Laplace transform; indenter; Hankel transform

INTRODUCTION

The determination of contact stresses, caused by non-stationary dynamic loading of elastic bodies, is one of the practically important problems in the theory of elasticity. The correct consideration of the influence of inertial forces on local deformations in the vicinity of the contact region is necessary for adequate simulation of the operation of a structure or mechanisms, in which components interact in a significant way at significant speeds. Microwave (ultrasonic) motors are typical examples of such mechanical systems. X. Tian *et al.* (2020) concluded that the principle

Suggested Citation:
Kutsenko, A., & Kutsenko, O. (2023). The gradual removal of Hertz pressure from the surface of elastic half-space. *Machinery & Energetics,* 14(4), 64-74. doi: 10.31548/machinery/4.2023.64.

*Corresponding author

of operation of some types of these devices is based on the transfer of kinetic energy from the stator to the rotor by contact forces arising in the process of their periodic collisions. Based on S.P. Wankhede & T.-B. Xu (2021), ultrasonic motors have been widely used in a variety of electronic devices due to their compactness, load torque at moderate rotation speeds and high positioning accuracy. They are widely used in the double-quick development of robotics (Toyama & Nishizawa, 2017). The simultaneous influence of surface and couple stresses on the non-symmetrical frictionless indentation of a linearly elastic, homogenous, and isotropic half-plane under a tilted, rigid, flat-ended indenter with sharp, square corners was investigated by T.M. Le *et al.* (2021) by adopting existing continuum-based models.

B. An *et al.* (2023) broadened the applicability of the vehicle-track dynamics model to account for 3D short-wave irregularities on rail surfaces. The key is developing a meshing grid approach combined with the accurate conjugate gradient (CG) method for contact mechanics under arbitrary 3D contact geometry. Therefore, both the global dynamics and local contact solutions can be provided. In this study, short-pitch rail corrugation is employed for investigating the role of 3D contact geometry in modelling dynamic wheel-rail interaction. The traditional vehicle-track coupled dynamics model using Hertzian spring is used for comparison. The results show that short-pitch rail corrugation contributes two different aspects, i.e., wheel centre trajectory and time-varying contact stiffness. These two aspects are found to be the root causes for explaining the influence of the varying 3D geometry irregularity size on dynamic wheel-rail contact force.

Accounting for the processes that occur during the dynamic contact interaction of solids is also important in the development and design of "classical" machinery. An example is the operation of various crushing machines which were described by B. Doroszuk & R. Król (2022), and Z. Chen *et al.* (2021). In particular, for processing agricultural products, the mechanisms, such as grinding mills, are used. To describe the operation of the crusher more accurately, X. Lv *et al.* (2021), I. Kupchuk *et al.* (2022) addressed the wave processes that occur when parts of the mechanism interact with the crushed material. Many scientists considered similar problems in Ukraine. In particular, the study of V.A. Bazhenov & M.O. Vabishchevich (2020) is relevant to the branch of construction. Similar studies were conducted by V.G. Popov & A.I. Kirillova (2020) in the field of mechanical engineering.

H. Xie *et al.* (2022) noted that the dynamic interaction of a rigid sphere with an elastic half-space should be considered using recently developed particle dynamics. From the provisions of this theory, J. Zhao *et al.* (2021) established that the problem was reduced to a wave equation concerning one of the components of the displacement vector. Based on the mentioned solution, a plausible conclusion was made on the similarity at any time of the distribution of contact stresses to Hertz's distribution. However, the conclusion that the maximum pressure according to

Hertz's theory is much less than the calculated holds unresolved issues. According to the given relations, their correlation depends only on Poisson's ratio of the material of the half-space and does not depend on the initial velocity of the sphere. When Poisson's ratio changes from 0 to 0.5, this relation changes from 0.74 to 0.

Thus, it can be concluded that the presented results of previous studies contain several contradictions. Therefore, with the solution to this sort of issue, various numerical methods were used, the finite element method being used most often (Lee & Komvopoulos, 2018; Habchi, 2018). This is also facilitated by the fact that in modern finite element packages, both commercial and freely available, the various algorithms of the contact interaction of finite elements are implemented. However, based on numerical solutions, it is difficult to restore the analytical dependence of the process characteristics on the values of the input parameters. Despite the already fairly long history of research, the important problem of estimation of the contact interaction of the surface of the body under study with measure sensors is open still. Hence, the study aims to determine the energy remainder that causes waves in the case of a contact problem.

MATERIALS AND METHODS

The distribution of normal displacements of surface points under gradual loading of a half-space with a load, according to Heasrtz's law was obtained by using the solution to the corresponding problem of instantaneous loading. Therefore, to present the solution to the problem of gradual loading in a closed form and simplify the perception of the material, the main results of a study by A.G. Kutzenko *et al.* (2001) were employed, which addressed the loading of a half-space by the Hertz's pressure. The elastic half-space $z < 0$ was considered, which at time $t < 0$ had been in static equilibrium, and its surface was not loaded. At the moment of time $t = 0$, the pressure, that was given by Hertz's contact theory, was instantly applied to the surface of the half-space in a circular domain $0 \leqslant r \leqslant a$ (Fig. 1).
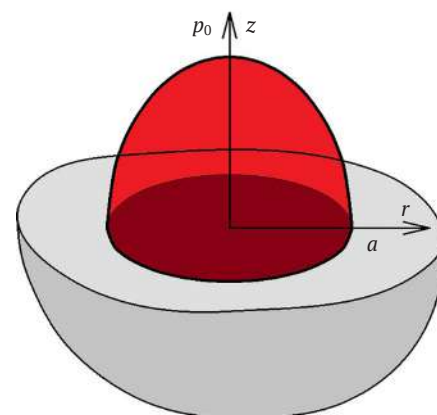

Figure 1. Loading of the elastic half-space by Hertz's pressure

Note: *a – load area radius; z, r – spatial coordinates; p_0 — pressure magnitude*

This pressure was considered a constant variable in the study. It was used to determine the normal displacements of the surface points of the half-space, as a function of time t and radial coordinate r. This was an additional task. The corresponding initial and boundary conditions were formulated as follows:

$$w|_{t=0} = u|_{t=0} = 0, \left.\frac{\partial w}{\partial t}\right|_{t=0} = \left.\frac{\partial u}{\partial t}\right|_{t=0} = 0, \quad (1)$$

and

$$\tau_{rz}|_{z=0} = 0, \ \sigma_r|_{z=0} = H(t)\begin{cases}-p_0\sqrt{1-r^2/a^2}, & r < a, \\ 0, & r > a,\end{cases} \quad (2)$$

where w, u – thickness (normal) and radial (tangential) displacements of the points of the half-space; σ_r, τ_{rz} – normal and shear stresses on the surface of a half-space; $H(t)$ – Heaviside function.

The maximum contact pressure was an independent parameter in the boundary conditions (2). However, considering the further extension of the results to cases of gradual loading of a half-space, it was expressed according to Hertz's theory in terms of the radius of the load area a and the radius of curvature of the equivalent indenter R:

$$p_0 = \frac{4Ga}{\pi(1-\nu)R}, \quad (3)$$

where G – shear modulus, ν – Poisson's ratio of the half-space material. All three parameters p_0, a, and R were considered as constant variables in the study. Only one parameter R was considered as a constant in the gradual load issue, as parameters p_0 and a were changed with time.

If the Laplace transform L with was applied concerning time and the Hankel transform H to the spatial coordinate r to Lamé equations of motion respectively, displacements can be represented as multiple integrals of the Riemann-Mellin inversion:

$$w(r,z,t) = \frac{1}{2\pi i}\int_0^\infty J_0(\lambda r)\lambda d\lambda \int_{\delta-i\infty}^{\delta+i\infty} W(\lambda,z,s)\exp(st)ds,$$
$$u(r,z,t) = \frac{1}{2\pi i}\int_0^\infty J_1(\lambda r)\lambda d\lambda \int_{\delta-i\infty}^{\delta+i\infty} U(\lambda,z,s)\exp(st)ds. \quad (4)$$

In this case, the images $W(\lambda,z,s)$ and $U(\lambda,z,s)$ satisfied the system of differential equations:

$$\kappa\frac{d}{dz}\left(\frac{dW}{dz}+\lambda U\right) - \lambda\left(\frac{dU}{dz}+\lambda W\right) = \frac{s^2}{c_2^2}W,$$
$$-\kappa\lambda\left(\frac{dW}{dz}+\lambda U\right) + \frac{d}{dz}\left(\frac{dU}{dz}+\lambda W\right) = \frac{s^2}{c_2^2}U, \quad (5)$$

where $\kappa = 2\frac{1-\nu}{1-2\nu} = \frac{c_1^2}{c_2^2} > 1, c_1 = \sqrt{2\frac{1-\nu}{1-2\nu}\frac{G}{\rho}}, c_2 = \sqrt{\frac{G}{\rho}}$ – the velocities of propagation of tension-compression waves and shear waves, respectively.

The zero initial conditions (1) were considered when equation (5) was deriving. To satisfy the boundary conditions (2), the Laplace and Hankel transformations were also applied:

$$\left.\left(\frac{1-\nu}{1-2\nu}\frac{dW}{dz}+\frac{\nu\lambda}{1-2\nu}U\right)\right|_{z=0} = -\Pi_0(\lambda,s), \left.\left(\frac{dU}{dz}-\lambda W\right)\right|_{z=0} = 0, (6)$$

where

$$\Pi_0(\lambda,s) = \Pi_0^i(\lambda,s) = -\mathbf{L}\big(\mathbf{H}(\sigma_z|_{z=0})\big) =$$
$$= \frac{2}{\pi(1-\nu)R}\frac{\sin a\lambda - a\lambda\cos a\lambda}{s\lambda^2}. \quad (7)$$

The general solution of system (4), which satisfies the conditions of boundedness at infinity, was represented as:

$$W(\lambda,z,s) = \lambda\left(\frac{c_2}{s}\right)^2[-\kappa\gamma_1 A\exp(\lambda\gamma_1 s) + B\exp(\lambda\gamma_2 s)],$$
$$U(\lambda,z,s) = \lambda\left(\frac{c_2}{s}\right)^2[\kappa A\exp(\lambda\gamma_1 s) - \gamma_2 B\exp(\lambda\gamma_2 s)]. \quad (8)$$

Submitting it to conditions (6), the expression for the image of normal displacement of boundary points was obtained:

$$\widetilde{W}^i(\lambda,s,a) = W^i(\lambda,0,s) = -\Pi_0^i(\lambda,s)\frac{\gamma_1(\gamma_2^2-1)}{2\Delta} =$$
$$= \frac{1}{\pi(1-\nu)R}\frac{\gamma_1(\gamma_2^2-1)}{2\Delta}\frac{\sin a\lambda - a\lambda\cos a\lambda}{s\lambda^2}, \quad (9)$$

where $\gamma_1 = \sqrt{1+s^2/(c_1\lambda)^2}, \gamma_2 = \sqrt{1+s^2/(c_2\lambda)^2}$,

$\Delta = \Delta(s/\lambda) = \frac{(\gamma_2^2+1)}{4} - \gamma_1\gamma_2$ – Rayleigh determinant. Its single-valued branch was distinguished on the complex plane s by cutting, as shown in Figure 2.
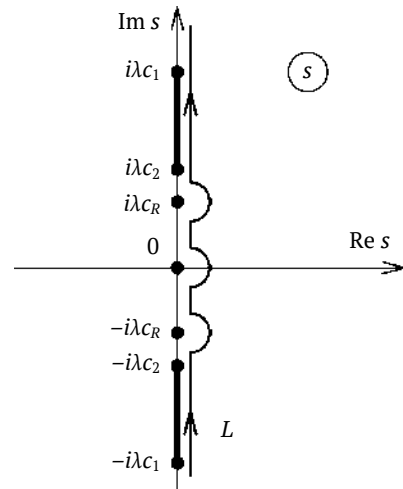

Figure 2. Integration contour
in the inverse Laplace transform
Note: c_R – the Rayleigh wave velocity; $s = \pm i\lambda c_R$ are poles of the function W

The radical branches γ_1 and γ_2 were chosen so that their values on the real axis s coincided with the values of the corresponding arithmetic roots. Such selection was used to obtain a representation of the solution in the form of a superposition of waves propagating from the surface into the depths of the half-space, and to ensure that the stress and displacement were clamped at $z\to-\infty$. The index "i" in expressions (7) and (9) indicated that the characteristic marked by it corresponded to the problem of *instantaneous* loading.

Since the points of the surface corresponded to a certain (zero) value of the coordinate z, i.e., normal displacements depended only on the variables r and t, this fact in (9) and below was denoted by the symbol "~". In addition, functions, containing the symbol "~" in their designation, were also considered as functions of the parameter a, necessary in the case of gradual loading of the half-space.

Further transformation (9) involved the inversions of the Laplace and Hankel transformations by (4). It was easy to verify that all singular points of expression (9) in the complex plane s stayed within the imaginary axis. According to the selection of branches of the radicals γ_1 and γ_2, the poles corresponded only to the points $s = 0$ and $s = \pm i\lambda c_R$, where c_R was the Rayleigh wave velocity. Therefore, function (9) was an analytic function of a variable parameter s in the right half-plane $Re\ s > 0$, which was used to shift the Laplace inversion contour to the imaginary axis.

Going around the poles of the function W, it was necessary to explicitly select the semi-residues equal to the integrals over the arcs of circles (Fig. 2). Performing this operation and introducing a new integration variable $x = -s_2 / (c_2\lambda)^2$, after the pairwise union of the integrals corresponding to the upper and lower parts of the axis $Im\ s$, the normal displacements of points on the surface of the half-space was represented in a form that does not contain complex variables:

$$\widetilde{w}^i(r,t,a) = -\frac{a^2}{\pi(1-v)R}f(\rho,\tau), \qquad (10)$$

where:

$$f(\rho,\tau) = (1-v)I(\rho) + \frac{1}{4\pi}\left\{\pi\frac{(1-q/2)^2\sqrt{1-q/\kappa}I_C(l,2r)}{(1-q/2)^3-(1+\kappa^{-1}-2q/\kappa)/2} - \right.$$
$$-\int_0^1\frac{\sqrt{1-x/\kappa}I_S(\rho,2\tau\sqrt{x/q})}{(1-x/2)^2-\sqrt{(1-x/\kappa)(1-x)}}dx -$$
$$-\int_0^\infty\frac{\sqrt{x/\kappa-1}I_C(\rho,2\tau\sqrt{x/q})}{(1-x/2)^2+\sqrt{(x/\kappa-1)(x-1)}}dx - \qquad (11)$$
$$-\int_1^\kappa\frac{(1-x/\kappa)^2\sqrt{1-x/\kappa}I_S(\rho,2\tau\sqrt{x/q})}{(1-x/2)^4-(1-x/\kappa)(1-x)}dx -$$
$$\left.-\int_1^\kappa\frac{(1-x/\kappa)\sqrt{x-1}I_C(\rho,2\tau\sqrt{x/q})}{(1-x/2)^4-(1-x/\kappa)(1-x)}dx\right\}.$$

The dimensionless independent variables $\rho = r/a$ and $\tau = (c_R t)/a$ were introduced in the expressions (10)-(11), as well as a parameter $q = c_R^2/c_2^2$ – the square of the ratio of the Rayleigh wave velocity to the shear wave velocity, which was a simple pole of the integrand of the first integral in (11). The index "i" at $\widetilde{w}$ indicated, as before, that this distribution of normal displacements corresponded to the problem of *instantaneous* loading. After relocation of the contour of the inverse Laplace transform to the imaginary axis, the integrals of the inverse Hankel transform I, I_S, and I_C were as follows:

$$I(\rho) = \left(1-\frac{\rho^2}{2}\right)I_1(\rho) + \frac{I_2(\rho)}{2},$$
$$I_S(l,\xi) = \left(1-\xi^2-\frac{\rho^2}{2}\right)I_{S1}(l,\xi) + \frac{I_{S2}(l,\xi)}{4}, \qquad (12)$$
$$I_C(l,\xi) = \left(1-\xi^2-\frac{\rho^2}{2}\right)I_{C1}(l,\xi) + \frac{I_{C2}(l,\xi)}{4},$$

where:

$$I_1(\rho) = \begin{cases} \pi/2, \rho \leq 1, \\ arcsin\ \rho^{-1}, \rho \geq 1, \end{cases}$$

$$I_{S1}(\rho,\xi) = \frac{1}{2}\begin{cases} ln\left(1+\xi+\sqrt{(1+\xi)^2-\rho^2}\right) - ln\left(|1-\xi|+\sqrt{(1-\xi)^2-\rho^2}\right), \quad |1-\xi| \geq \rho, \\ ln\left(1+\xi+\sqrt{(1+\xi)^2-\rho^2}\right) - ln\ \rho, \quad |1-\xi| \leq \rho \leq 1+\xi, \\ 0, \quad 1+\xi \leq \rho, \end{cases} \qquad (13)$$

$$I_{C1}(\rho,\xi) = \frac{1}{2}\begin{cases} \pi H(1-\xi), \quad |1-\xi| \geq \rho, \\ \pi/2 + arcsin((1-\xi)/\rho), \quad |1-\xi| \leq \rho \leq 1+\xi, \\ arcsin((1+\xi)/\rho) + arcsin((1-\xi)/\rho), \quad 1+\xi \leq \rho \end{cases}$$

and

$$I_2(\rho) = \begin{cases} 0, \rho \leq 1, \\ \sqrt{\rho^2-1}, \rho \geq 1, \end{cases}$$

$$I_{C2}(\rho,\xi) = \begin{cases} 0, \quad |1-\xi| \geq \rho, \\ (1+3\xi)\sqrt{\rho^2-(1-\xi)^2}, \quad |1-\xi| \leq \rho \leq 1+\xi, \\ (1+3\xi)\sqrt{\rho^2-(1-\xi)^2} + (1-3\xi)\sqrt{\rho^2-(1+\xi)^2}, \quad 1+\xi \leq \rho, \end{cases} \qquad (14)$$

$$I_{S2}(\rho,\xi) = \frac{1}{2}\begin{cases} sign(1-\xi)(1+3\xi)\sqrt{(1-\xi)^2-\rho^2} - (1-3\xi)\sqrt{(1+\xi)^2-\rho^2}, \quad |1-\xi| \geq \rho, \\ -(1-3\xi)\sqrt{(1+\xi)^2-\rho^2}, \quad |1-\xi| \leq \rho \leq 1+\xi, \\ 0, \quad 1+\xi \leq \rho. \end{cases}$$

The plots of displacements found based on (10) for various values of the dimensionless time are shown in Figure 3. The analysis highlighted the reason for the selection of Rayleigh as the characteristic velocity in the nondimensionalization of time. This velocity determined the dynamics of transient processes under instantaneous loading of the half-space. After the propagation of the Rayleigh wave excited at the point of the loading area, which is the most distant from the given point of the half-space surface, the static value of the normal displacement was instantly set in the latter one. This important property was used in further transformations.
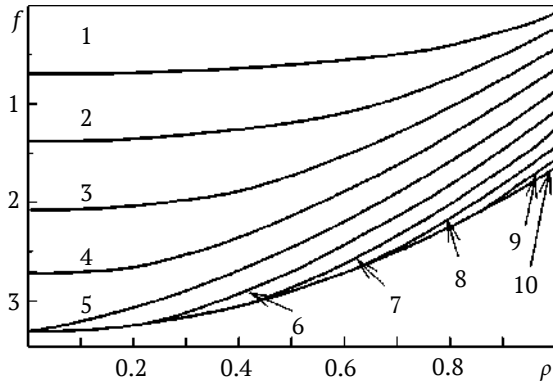
Figure 3. Dimensionless function $f(\rho, \tau)$ for $\nu = 0.3$
at moments of dimensionless time $\tau = n/10$,
where n is the number of the curve
Source: developed by the authors

An elastic half-space that was at the initial moment $t = 0$ in an unloaded state of static equilibrium was used. At the given moment an area arises on its surface and then continues to grow, on which the pressure is distributed according to the law:

$$p(r,t) = p_0(t)\sqrt{1 - r^2/a^2(t)}, r \leq a(t), t > 0, \quad (15)$$

where $a = a(t)$ is the radius of the loading area. It was the time-respecting variable parameter. In this case, as before, the relation (3) determined the dependence of the maximum pressure $p_0(t)$ on the radius of the loading area. It was required to determine the time evolution of normal displacements on the surface of a half-space.

Since the initial conditions (1) and the first of the boundary conditions (2) were still true, the course of the solution to the given problem did not differ from the aforementioned, until the rest of the boundary conditions were satisfied. The main difference between the boundary conditions concerning the normal component of the stress vector in the problem of instantaneous and in the problem of gradual loading of a half-space was its significant time dependence in the second case. In this case, it was impossible to explicitly run the direct Laplace transform without the specification of the loading area radii dependence concerning time. Therefore, in the general case, instead of (7) and (9), the following was true:

$$\Pi_0(\lambda, s) = \Pi_0^g(\lambda, s) = -L\big(H(\sigma_z|_{z=0})\big) =$$

$$= -\frac{2}{\pi(1-\nu)R\lambda^3} \int_0^\infty (\sin a\,(\bar{t})\lambda - a(\bar{t})\lambda \cos a\,(\bar{t})\lambda) exp(-s\bar{t})d\bar{t}, (16)$$

and

$$\tilde{W}^g(\lambda, s) = -\frac{2}{\pi(1-\nu)R} \frac{\gamma_1(\gamma_2^2-1)}{\lambda^3 \Delta} \times$$

$$\Bigg\langle \int_0^\infty \binom{\sin a\,(\bar{t})\lambda -}{-a(\bar{t})\lambda \cos a\,(\bar{t})\lambda} exp(-s\bar{t})d\bar{t}. \quad (17)$$

The index "g" implied that the images of surface pressure and normal displacement correspond to *the gradual* loading of the half-space. It was necessary to apply the inverse Laplace and Hankel transformations to (17)

following the first relation in (4) to find the expression of normal displacements. In the general case, it was impossible to run the corresponding integration since the form of the function W itself was unknown. However, since only one of these integrals was singular, they could be introduced under the sign of the integral contained on the right side of (17), i.e., the order of integration could be changed (Gakhov, 2014). Hence, such a permutation could be used to reduce the procedure of taking the internal integrals of the Riemann-Mellin inversion to the calculations made above. It should be remembered that the radius $a(\bar{t})$ acts as an independent parameter in internal integrals. Therefore, the inversion integrals were obtained from the product of the function $\tilde{W}^i(\lambda, s, a)$ and the parameters. The last multiplier is explained by the absence of the Heaviside function in the boundary conditions under gradual loading. In addition, the exponent of the Laplace inversion kernel contained the difference $t - \bar{t}$ instead of t, which was derived as a result of a rearrangement of the order of integration. Thus, the following was true:

$$\tilde{w}^g(r,t) = \frac{1}{2\pi i} \int_0^\infty d\bar{t} \int_0^\infty J_0(\lambda r)\lambda d\lambda$$
$$\int_{\delta-i\infty}^{\delta-i\infty} \tilde{W}^i(\lambda, s, a(\bar{t}))s \, exp\big(s(t - \bar{t})\big) ds. \quad (18)$$

The theorem on differentiation of the Laplace transformation original to (18) was applied and $\tilde{w}^i(r,t,a) \equiv 0$ was implied for $t \leqslant 0$, to derive the following:

$$\tilde{w}^g(r,t) = \int_0^t \frac{\partial \tilde{w}^i(r,t-\bar{t},a(\bar{t}))}{\partial t} d\bar{t}. \quad (19)$$

It expressed the normal displacements under gradual loading of the half-space in terms of the normal velocities of the surface points under its instantaneous loading. The relationship (19) could be obtained from simpler considerations, based on the incremental approach. Therefore, the process of continuous loading was replaced by a step change in surface pressure at discrete moments separated from each other by a small time interval Δt. A loading area with radius $a_1 = a(t_1)$ was assumed to have arisen on the surface of the half-space at the moment of time $t_1 = \Delta t$. The normal displacements of points on the surface of the half-space were described until the next moment of load change by the expression:

$$\tilde{w}^s(r,t) = \tilde{w}^i(r, t - t_1, a_1), t_1 < t < t_2, \quad (20)$$

where the index "s" denoted stepwise load change. At the moment of time $t_2 = t_1 + \Delta t$, the radius of the loading area changed abruptly from a_1 to $a_2 = a(t_2)$. It corresponded to instantaneous load removal along the area with the radius a_1 and instantaneous application along the area with radius a_2 at $t = t_2$:

$$\tilde{w}^s(r,t) = \tilde{w}^i(r, t-t_1, a_1) - \tilde{w}^i(r, t-t_2, a^1) + \tilde{w}^i(r, t-t_2, a_2),$$
$$t_2 < t < t_3. \quad (21)$$

The following obtained expression for normal displacements at the N-th step is as follows:

$$\tilde{w}^s(r,t) = \tilde{w}^i(r, t - t_{N+1}, a_{N+1}) +$$
$$+ \sum_{k=1}^{N} \left[\tilde{w}^i(r, t - t_k, a_k) - \tilde{w}^i(r, t - t_{k+1}, a_k) \right] \approx$$
$$\approx \tilde{w}^i(r, t - t_{N+1}, a_{N+1}) + \sum_{k=1}^{N} \frac{\partial \tilde{w}^i(r, t - t_k, a_k)}{\partial t} \Delta t,$$
$$t_N < t < t_{N+1}. \tag{22}$$

When the parameter Δt was zero in expression (22), the expression (19) was used instead. In the case when a static load was applied along the radius a_0 to the surface of the half-space, two more terms would be added to the integral on the right side of (19):

$$\tilde{w}^H(r, a_0) \text{-} \tilde{w}^i(r, t, a_0). \tag{23}$$

The first of them described the field of normal displacements in the Hertz contact problem:

$$\tilde{w}^H(r, a_0) = -\frac{2a_0^2}{\pi R} I\left(\frac{r}{a_0}\right). \tag{24}$$

The second term corresponded to the removal of this load at the initial moment. Therefore, the expressions for normal displacements during gradual loading of the half-space due to normal velocities of surface points during its instantaneous loading and normal displacements in contact interaction were obtained.

RESULTS AND DISCUSSION

The relationship (19), addressing (23), was utilised to consider the evolution of normal displacements for different laws of change in the radius of the loading area $a = a(t)$. However, this study only focused on the case when the dependence of the radius of the loading area on time is a monotonically decreasing function, which corresponds to the process of unloading the half-space (Fig. 4).
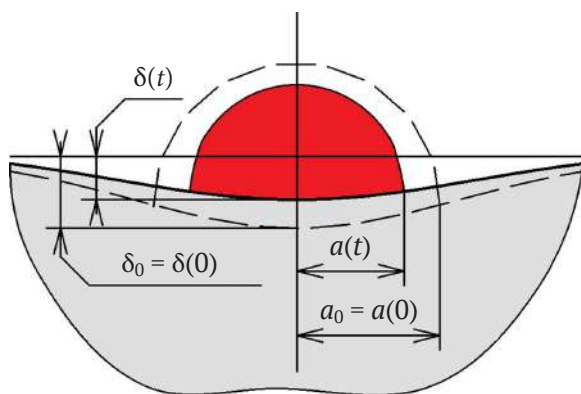

Figure 4. The gradual unloading
of the elastic half-space
Note: $a = a(t)$ is the radius of the loading area; $\delta = \delta(t)$ – the law of change in the penetration depth of an equivalent indenter; δ_0 – the initial value of the depth of the penetration
Source: developed by the authors

In this case, to achieve the goals formulated in the introduction, it is sufficient to determine the function (11) and its partial derivative only at $\rho < 1$, since only the normal displacements of points that currently belong to the loading area are considered in this study. In practice, it is better to set not the law of change in the radius of the contact area, but the law of change in the penetration depth of an equivalent indenter δ, which, following the Hertz's theory, is related to the radius by the relation:

$$\delta = a^2/R. \tag{25}$$

Three partial dependencies $\delta = \delta(t)$ will be considered, namely $\delta = \delta_0(1\text{-}t/T)$ – uniform unloading, $\delta = \delta_0(1\text{-}(t/T)^2)$ – uniformly accelerated unloading and $\delta = \delta_0 cos(\pi t/((2T)))$. The last expression accurately approximates the dependence, which follows from Hertz's quasi-static contact theory, of the penetration depth as a function of time during the collision of two elastic balls moving by inertia (Johnson, 2012). Here, δ_0 is the initial value of the depth of the penetration, and T is the period of unloading. In the case of unloading, relation (19) can be represented in a dimensionless form considering (23):

$$\pi \frac{\tilde{w}^g(r,t)}{\delta_0} = -2I(\rho) + \frac{1}{1-\nu}\left[f(\rho, \tau) - \int_0^\tau d(\bar{\tau}) f_\tau\left(\frac{\rho}{d(\bar{\tau})}, \frac{\tau - \bar{\tau}}{d(\bar{\tau})}\right) d\bar{\tau}\right],$$
$$\tau < \tau_{max}, \tag{26}$$

where

$$\rho = \frac{r}{a_0} = \frac{r}{\sqrt{R\delta_0}}, \tau = \frac{c_R t}{2a_0} = \frac{c_R t}{2\sqrt{R\delta_0}},$$
$$d(\tau) = \sqrt{\frac{\delta(t)}{\delta_0}} = \sqrt{\frac{\delta(2\tau\sqrt{R\delta_0}/c_R)}{\delta_0}},$$
$$f_\tau(\rho, \tau) = \frac{\partial f(\rho, \tau)}{\partial \tau}, \ \tau \frac{c_R T}{2\sqrt{R\delta_0}}_{max}. \tag{27}$$

During the calculation of the function value, the order of the integration and derivation operations in (11) can be changed and performed analytically. Thus, the determination of f_τ values is reduced to simple (not multiple) integrations, similar to those that arise when calculating the antiderivative of function f. A three-dimensional plot of $-f_\tau(\rho, \tau)$ on the square $[0,1] \times [0,1]$ is shown in Figure 5.
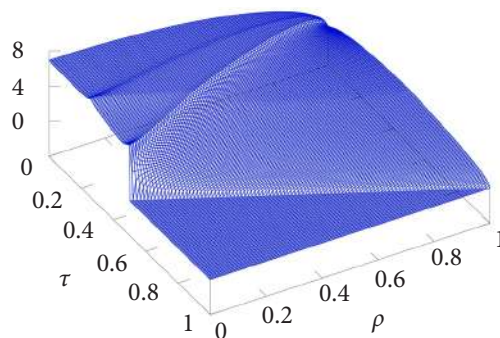

Figure 5. Surface $-f_\tau(\rho, \tau)$ for $\nu = 0.3$
Source: developed by the authors

Figure 6 shows a plot of the same function but in the form of isolines. As can be seen, this function is bounded and continuous everywhere, except for the point $\rho = 0$, $\tau = 1/2$, where a finite gap is present along the axis τ. The advantage of representation (26) in comparison with other possible methods for the solution of the problem of gradual loading/unloading of a half-space is explained by the fact that, in addition to dimensionless variables, the function f_τ depends only on the Poisson ratio as a parameter and can be easily tabulated. Thus, the calculation following (26) is reduced to the integration of a bounded, continuous function.
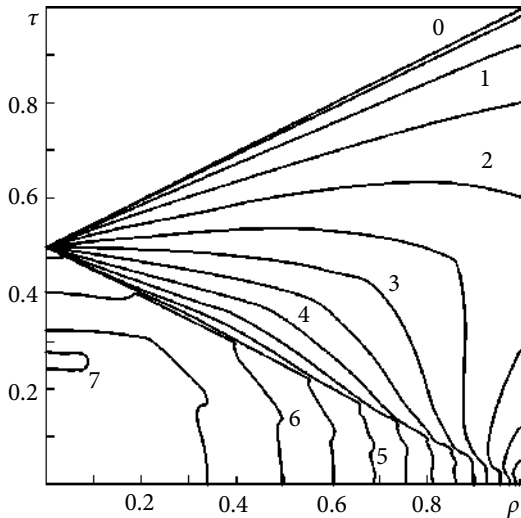

Figure 6. The isolines
of a dimensionless function $-f_\tau(\rho, \tau)$
Note: the values of the function are indicated near the isoline
Source: developed by the authors

The representation (26) also shows that the only parameter significant for the process, in addition to the Poisson ratio, is the dimensionless period of unloading τ_{max}, which is equal to the number of diameters of the initial loading area that the Rayleigh wave travels during the unloading time. In addition, based on (26), for random dependence $d = d(\tau)$, which is monotonically decreasing to zero, it can be proved that in the limiting case, when τ_{max}, the distribution of normal displacements tends to the distribution given by Hertz's theory for the current value of the penetration depth. The depth of penetration ($d = \sqrt{1 - \tau/\tau_{max}}$) when $\tau > 1$ is demonstrated in the example of the linear law of decreasing. In this case, the first two terms on the right side of (26) on the loading area completely compensate for each other. However, $f_\tau(\rho, \tau) \neq 0$ at $\rho \leqslant 1$, when $\tau < 1$. Considering the dependence $d = d(\tau)$, it is possible to conclude that the integrand in the remaining term is nonzero on a narrow interval $\tau_1 < \bar{\tau} < \tau$, where

$$\tau_1 = \tau - \frac{1}{2\tau_{max}}\sqrt{1 - \frac{\tau}{\tau_{max}} + \frac{1}{4\tau_{max}^2}} \approx \tau - \sqrt{1 - \frac{\tau}{\tau_{max}}}.$$

Hence, $d(\bar{\tau}) \approx d(\tau)$ and:

$$\pi \frac{\tilde{w}^g(r,t)}{\delta_0} \approx \frac{d(\bar{\tau})}{1-\nu}\left[\int_0^\tau f_\tau\left(\frac{\rho}{d(\bar{\tau})}, \frac{\tau - \bar{\tau}}{d(\bar{\tau})}\right) d(\bar{\tau})\right]. \quad (28)$$

Running the integration in (28), the required results are obtained. It also follows from the above reasons that the magnitude of the deviation of the displacements caused by the gradual removal of the load from Hertz quasi-static displacements is of the order of τ_{max}^{-1}.

Figures 7-10 show the distributions of the displacements "under the indenter", which were calculated using linear (26) (Fig. 7 and 8) and quadratic (Fig. 9 and 10) unloading laws corresponding to different speeds. For comparison analysis, the dashed lines indicate the surface profiles of the loading area given by Hertz's theory for the corresponding penetration depth of the indenter.

Each pair of solid and dashed curves corresponds to a fixed time $0 < \tau < \tau_{max}$. For example, in Figure 7, which corresponds to constant indent speed and τ_{max} the five such pairs for time points $\tau = 1$, $\tau = 3$, $\tau = 5$, $\tau = 7$ and $5 \to \tau = 9$ are represented. The lengths of curves decrease with time as the size of the load area also decreases. This fact is indicated by the upper dashed outline. The lower dashed contour corresponds to the distribution of displacements in Hertz's static contact problem. The curves in each pair are similar, only slightly shifted relative to each other in the vertical direction. In other words, there is an almost constant vertical gap between them. This gap means that the dynamic distribution of normal displacements lags behind the quasi-static Hertzian distribution. Moreover, for a constant speed of removing the indentor, this lag decreases until the end of the unloading process.

A comparison of Figures 7 and 8 (the latter also shows data for a constant indenter speed but with τ_{max}) indicates that with an increase in the indenter speed, the difference between the dynamic and quasi-static distributions increases.
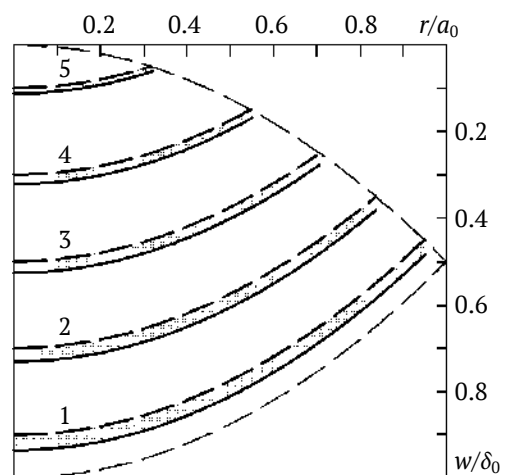

Figure 7. The normal displacements of points of loading
area for the law $\delta = \delta_0 (1 - \tau/10)$
Note: $1 \to \tau = 1$, $2 \to \tau = 3$, $3 \to \tau = 5$, $4 \to \tau = 7$, $5 \to \tau = 9$
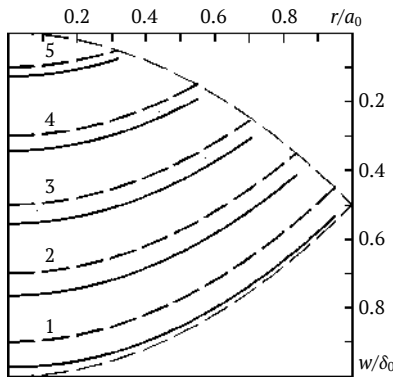**Source:** developed by the authors

Figure 8. The normal displacements of points
of loading area for the law $\delta = \delta_0 (1 - \tau/5)$
Note: $1 \rightarrow \tau = 0.5$, $2 \rightarrow \tau\ 1.5$, $3 \rightarrow \tau = 2.5$, $4 \rightarrow \tau = 3.5$, $5 \rightarrow \tau = 4.5$
Source: developed by the authors

This conclusion remains valid even with uniformly accelerated movement of the indenter (see Fig. 9 and 10). Only in this case, the gap between the distributions increases until the end of the unloading process. A similar behaviour of the deviations of normal displacements is also characteristic of the dependence $\delta = \delta_0 \cos(\pi\tau/(2\tau_{max}))$, except that in the last case in the second half of the unloading period, there is a noticeable tendency to their decrease.
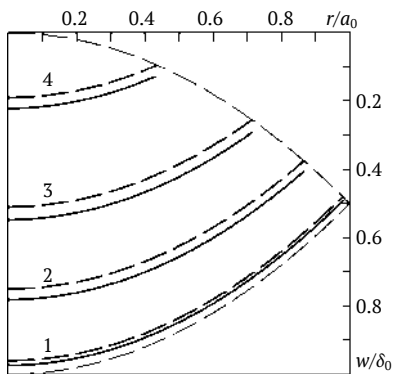

Figure 9. The normal displacements of points
of loading area for the law $\delta = \delta_0 (1 - \tau/10)^2$
Note: $1 \rightarrow \tau = 2$, $2 \rightarrow \tau = 5$, $3 \rightarrow \tau = 7$, $4 \rightarrow \tau = 9$
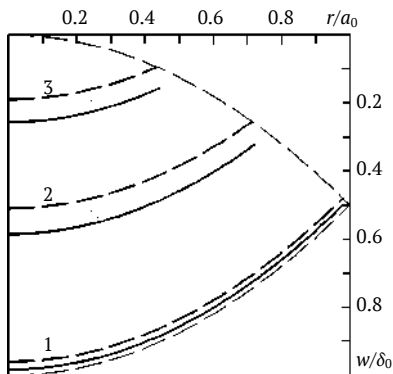**Source:** developed by the authors

Figure 10. The normal displacements
of points of loading area for the law $\delta = \delta_0 (1 - \tau/5)^2$
Note: $1 \rightarrow \tau = 1$, $2 \rightarrow \tau = 3.5$, $3 \rightarrow \tau = 4.5$
Source: developed by the authors

As expected, the deviations between quasi-static movements and movements caused by the gradual removal of the load increase with a decrease in the period of unloading. However, another regularity is noteworthy: at any fixed moment, these deviations are practically independent of the radial coordinate, i.e., the surface profile upon gradual removal of the load repeats the profile of an imaginary stamp, but at a slightly greater depth, depending on time. The latter suggests that by reducing the amplitude of surface forces, but leaving their distribution along the radial coordinate unchanged, it is possible to achieve a match between quasi-static and dynamic displacements. Setting instead of (15) the pressure in the form:

$$p(r,t) = kp_0(t)\sqrt{1 - r^2/a^2(t)}, r < a(t), t > 0, \quad (29)$$

It is necessary to select a coefficient from the condition of the least deviation of the displacement of the points of the surface of the half-space from the profile of the indenter.

Since the magnitude of the deviation varies with time, the coefficient k, in general, should be considered as a function of time. But for sufficiently long periods of unloading, a reasonable solution to the problem can be obtained, assuming that k is constant. In this case, this coefficient is the recovery coefficient during unloading of the half-space. The difference of $1 - k$ is the ratio of the energy carried away by elastic waves from the contact zone during unloading to the total initially accumulated energy of elastic deformation of the half-space.

The calculations were carried out for all three types of half-space unloading according to the proposed scheme. As a criterion for determination of the value of the coefficient k, the coincidence of the normal displacements of the half-space surface points and the corresponding indenter points averaged over the radius and over the complete unloading time was chosen, i.e.:

$$\int_0^T dt \int_0^{a(t)} \left(\widetilde{w}^g(r,t) - \widehat{w}^H(r, a(t)) \right) r dr = 0. \quad (30)$$

As such, the value depends not only on the dimensionless period of unloading τ_{max} but also on its nature. For the linear law of change in the depth of penetration the coefficient k is equal:

$$k \approx \frac{0,6}{\tau_{max}}, \quad (31)$$

for the other two laws, it is equal:

$$k \approx \frac{0,4}{\tau_{max}}, \quad (32)$$

(in the case of uniformly accelerated unloading, the value is slightly less than in the case of inertial movement of the indenter). It should be noted that expressions (31)-(32) make sense only for sufficiently large periods of unloading ($\tau_{max} \geq 10$). Otherwise, even for the optimal value, the deviations at certain points in time become comparable with the magnitudes of the displacements themselves.

However, the dimensionless contact period τ_{max} is inversely proportional to the ratio of the speed of insertion/

removal of an imaginary indenter and the speed of elastic waves in elastic space c_0. Therefore, the results obtained qualitatively coincide with those known from the literature, for example, those obtained by I.I. Argatov (2012), stating that the part of the energy spent on the formation of elastic waves increases with increasing this ratio. I.I. Argatov (2012) carried out an asymptotic analysis of the interaction of an elastic half-space with a slowly moving rigid spherical indenter. The superseismic and subsonic phases of interaction were considered separately. For each of them, the expressions for maximum penetration, contact time, and contact force dependence on time are derived. Based on the obtained relations, the above statement on the negligence of the superseismic phase can be questioned.

Therefore, the conclusion reached by H. Xie *et al.* (2022) on the independence of the maximum pressure from the indenter speed could be derived from the method used. At the same time, calculations of this study confirm the conclusion of K.L. Johnson (2012) on the insignificance of the contribution of the superseismic phase to the overall picture of contact interaction. Attempts of rectification of Hertz's theory for the case of dynamic contact were made repeatedly. An analysis of earlier studies was conducted by K.L. Johnson (2012). In particular, the time of the so-called super seismic phase, when the boundary of the contact area moves faster than elastic waves, was determined as negligible. In addition, it is noted that for indenter velocities of an order of magnitude lower than the elastic wave velocities in the half-space, the quasi-static Hertz theory gives a good approximation. The applicability criterion for such an approach, which is called Love's criterion, is given in the fundamental paper of K.L. Johnson (2012). According to this criterion, it has the following formulation: Hertz's theory approximates the real distribution of contact pressure more accurately, that the smaller the ratio of the approach (retreat) velocity of the bodies V to the characteristic value of the elastic wave velocities inside the bodies themselves c_0. The physical implication of this criterion determines that the more times the elastic waves return to the point of impact during the contact time (it is reflected from the distant boundaries of the bodies) the more the deformation process can be like static deformation. As K.L. Johnson (2012) pointed out, this criterion is true even if the dimensions of one of the bodies are so large that during the time of contact, the waves do not have time to return to the point of impact.

C. Zhao (2011), Y. Shen & V. Giurgiutiu (2014) proved that an example of the practical application of the results of dynamic contact mechanics was non-destructive ultrasonic testing and monitoring. However, the determination of contact stresses in the case of the exact formulation of the corresponding boundary value problems of the dynamic theory of elasticity is accompanied by overcoming some mathematical difficulties. H. Jalali & P. Rizzo (2021) concluded that one of the characteristic features of non-stationary contact problems is the dependence of the size, and sometimes the shape of the contact area concerning time, which cannot be deducted in advance. Y. Yang *et al.* (2019)

and Q. Peng *et al.* (2021) determined that the absence of relatively simple analytical expressions for contact stresses that consider local dynamic effects is the reason for the practically uncontested use of Hertz's quasi-static theory of impact in applied problems.

Thus, the obtained results of calculations and graphical dependencies obtained on their basis indicate that the gradual removal of the load from the surface of the elastic half-space has been achieved and the Hertzian pressure can be determined sufficiently accurately by the proposed method.

CONCLUSIONS

In the course of the research, an efficient method for calculating normal displacements in the area of loading during dynamic contact interaction of elastic bodies was developed. This method is based on exact solutions to non-stationary problems and holds practical significance for modelling structures operating at high velocities. The only significant parameter in the problem of gradual loading (unloading) of an elastic half-space, excluding the Poisson ratio of the material of the half-space, is the dimensionless loading (unloading) period τ_{max}, which is equal to the characteristic diameter of the loading area, which the Rayleigh wave travels during the loading (unloading) time. With a gradual removal of pressure, the normal displacements of the points of the loading area always lag behind the corresponding quasi-static values given by Hertz's theory, and this lag is proportional to τ_{max}^{-1} for large values of the dimensionless period of unloading. This phenomenon of inertia of points on the surface of the half-space leads to a decrease in the contact pressure compared to the Hertz pressure when the indenter is removed (it is logical to assume that when the indenter is deepened, the inertia of the surface of the half-space leads to an increasing in pressure). For sufficiently long periods of unloading ($\tau_{max} \geqslant 10$), the deviation of normal displacements from its quasi-static value is practically independent of the radial coordinate, i.e., uniform over the loading area, independently of the unloading law. For long periods of unloading, the ratio of the energy spent on the formation of elastic waves to the total energy of the initial elastic deformation is described by the expression $C\tau_{max}^{-1}$, where the constant value of C is different for different laws of unloading.

Considering the rapid development of computing tools, it seems promising to study this problem using the finite element method. This approach will not only allow us to compare numerical results but also suggest the time dependence of the penetration depth of a real, rather than imaginary, stamp. The latter, in turn, will make it possible to perform a more accurate assessment of the energy of elastic waves using the proposed analytical method.

CONFLICT OF INTEREST

None.

REFERENCES

[1] An, B., Sun, Y., Liu, J., Tao, G., Qian, Y., & Wang, P. (2023). The role of 3D contact geometry in modeling dynamic wheel-rail interaction at short-wave irregularities on rail surface. *Engineering Failure Analysis*, 153, article number 107559. doi: 10.1016/j.engfailanal.2023.107559.

[2] Argatov, I.I. (2012). Slow vertical motions of a spherical indenter on an elastic half-space. *Quarterly Journal of Mechanics and Applied Mathematics*, 65(1), 129-140. doi: 10.1093/qjmam/hbr023.

[3] Bazhenov, V.A., & Vabishchevich, M.O. (2020). Research of nonlinear dynamic deformation of spatial bodies with cracks. *Technology Audit & Production Reserves*, 2(1(52)), 16-23.

[4] Chen, Z., Wang, G., Xue, D., & Cui, D. (2021). Simulation and optimization of crushing chamber of gyratory crusher based on the DEM and GA. *Powder Technology*. 384, 36-50. doi: 10.1016/j.powtec.2021.02.003.

[5] Doroszuk, B, & Król, R. (2022). Industry scale optimization: Hammer crusher and dem simulations. *Minerals*, 12(2), article number 244. doi: 10.3390/min12020244.

[6] Gakhov, F.D. (2014). *Boundary value problems*. New-York: Elsevier.

[7] Habchi, W. (2018). *Finite element modeling of elastohydrodynamic lubrication problems*. Hoboken: John Wiley & Sons. doi: 10.1002/9781119225133.

[8] Jalali, H., & Rizzo, P. (2021). Numerical investigation of the interaction of highly nonlinear solitary waves with corroded steel plates. *International Journal of Mechanical Sciences*, 208, article number 106676. doi: 10.1016/j.ijmecsci.2021.106676.

[9] Johnson, K.L. (2012). *Contact mechanics*. Cambridge: Cambridge University Press. doi: 10.1017/CBO9781139171731.

[10] Kupchuk, I., Poberezhets, J., Kravets, R., & Lavreniuk, P. (2022). Energy intensity of the process of destruction of feed grain in conditions of dynamic contact interaction with the edge of the disc impactor. *Engineering, Energy, Transport AIC,* 117(2), 97-103. doi: 10.37128/2520-6168-2022-2-10.

[11] Kutzenko, A.G., Ulitko, A.F., & Oliynik, V. (2001). Displacements of the elastic half-space surface caused by instantaneous axisymmetric loading. *International Journal of Fluid Mechanics Research,* 28(1&2), 258-273. doi: 10.1615/InterJFluidMechRes.v28.i1-2.190.

[12] Le, T.M., Wongviboonsin, W., Lawongkerd, J., Bui, T.Q., & Rungamornrat, J. (2021). Influence of surface and couple stresses on response of elastic substrate under tilted flat indenter. *Applied Mathematical Modelling*, 104, 644-665. doi: 10.1016/j.apm.2021.12.013.

[13] Lee, A., & Komvopoulos, K. (2018). Dynamic spherical indentation of elastic-plastic solids. *International Journal of Solids and Structures,* 146, 180-191. doi: 10.1016/j.ijsolstr.2018.03.028.

[14] Lv, X., Su, J., Tian, J.-Y., & Ke, L.-L. (2021). Dynamic contact response of an elastic sphere on a piezoelectric half-space, *Applied Mathematical Modelling*, 100, 16-32. doi: 10.1016/j.apm.2021.07.012.

[15] Peng, Q., Liu, X., & Wei, Y. (2021). Elastic impact of sphere on large plate. *Journal of the Mechanics and Physics of Solids,* 156, article number 104604. doi: 10.1016/j.jmps.2021.104604.

[16] Popov, V.G., & Kirillova, A.I. (2020). Mathematical modeling of contact interaction under torsional oscillations. In *International Scientific and Technical Conference "Ship Electrical Engineering, Electronics and Automation"* (pp. 133-136). Odesa: National University "Odessa Maritime Academy".

[17] Shen, Y., & Giurgiutiu, V. (2014) Predictive modeling of nonlinear wave propagation for structural health monitoring with piezoelectric wafer active sensors. *Journal of Intelligent Materials Systems and Structure*. 25(4), 506-520. doi: 10.1177/1045389X13500572.

[18] Tian, X., Liu, Y., Deng, J., Wang, L., & Chen, W. (2020). A review on piezoelectric ultrasonic motors for the past decade: Classification, operating principle, performance, and future work perspectives. *Sensors and Actuators A: Physical*, 306, article number 111971. doi: 10.1016/j.sna.2020.111971.

[19] Toyama, S., & Nishizawa, U. (2017). Micro ultrasonic motor for miniature robot arm. *Vibroengineering PROCEDIA,* 13, 127-131. doi: 10.21595/vp.2017.18999.

[20] Wankhede, S.P., & Xu, T.-B. (2021). The roles of piezoelectric ultrasonic motors in industry 4.0 Era: Opportunities and challenges. *Piezoelectric Actuators – Principles, Design, Experiments and Applications*. doi: 10.5772/intechopen.100560.

[21] Xie, H., Zeng, Z., Su, M., Luo, J., & Dai, G. (2022). On mechanical and motion behavior of the normal impact interface between a rigid sphere and elastic half-space. *Applied Sciences*, 12(21), article number 11094. doi: 10.3390/app122111094.

[22] Yang, Y., Zeng, O., & Wan L. (2019). Dynamic response analysis of the vertical elastic impact of the spherical rock on the metal plate. *International Journal of Solids and Structures*, 158, 287-302. doi: 10.1016/j.ijsolstr.2018.09.017.

[23] Zhao, C. (2011). *Ultrasonic Motors*. Berlin: Springer. doi: 10.1007/978-3-642-15305-1.

[24] Zhao, J., Chen, S., Zhang, K., & Liu, Y. (2021). A review of many-body dissipative particle dynamics (MDPD): Theoretical models and its applications. *Physics of Fluids*, 33, article number 112002. doi: 10.1063/5.0065538.

Анастасія Григорівна Куценко
Кандидат фізико-математичних наук, доцент
Національний університет біоресурсів і природокористування України
03041, вул. Героїв Оборони, 15, м. Київ, Україна
https://orcid.org/0000-0003-1808-6773

Олексій Григорович Куценко
Кандидат фізико-математичних наук, доцент
Київський національний університет імені Тараса Шевченка
01033, вул. Володимирська, 60, м. Київ, Україна
https://orcid.org/0000-0001-5089-0409

Поступове зняття з поверхні пружного півпростору тиску Герца

Анотація. Визначення контактних напружень при нестаціонарному динамічному навантаженні пружних тіл має вирішальне значення для моделювання конструкцій при високих швидкостях, але це пов'язано з математичними труднощами через залежність від часу і часто невідомі розміри та форму контактної області. Основна мета роботи полягала в тому, щоб на основі точних розв'язків нестаціонарних задач для пружного півпростору отримати оцінку величини частини енергії, яка витрачається на утворення хвиль під час контактної взаємодії пружних тіл. Для цього за допомогою перетворення Ханкеля за радіальною координатою та перетворення Лапласа за часовою змінною реконструйовано розв'язок додаткової задачі – задачі про миттєве навантаження півпростору. Запропоновано метод знаходження переміщень у пружному півпросторі, який поступово навантажується (розвантажується) контактним тиском Герца. Його наявність дозволила перейти до розв'язання основної задачі – задачі поступового навантаження поверхні півпростору тиском Герца. Обґрунтовано можливість зміни порядку операцій диференціювання та інтегрування в отриманому представленні на основі властивостей підінтеграла. Розглянуто випадки, коли швидкість індентора постійна, коли його рух рівномірно прискорений і коли рух відповідає закону першої чверті періоду косинуса в часі. Зроблено висновок, що розподіл динамічних контактних напружень подібний до розподілу Герца. Зроблено оцінку частини енергії, що витрачається на формування пружних хвиль, для різних законів розвантаження. Практичне значення роботи полягає в розробці ефективного методу розрахунку нормальних переміщень на ділянці навантаження при динамічній контактній взаємодії пружних тіл, що може бути цінним для моделювання конструкцій, які працюють з високими швидкостями

Ключові слова: динамічна контактна взаємодія; уточнення контактного розподілу; енергія хвиль; перетворення Лапласа; штамп; перетворення Ханкеля